Assiut University Journal of Multidisciplinary Scientific Research (AUNJMSR)
Faculty of Science, Assiut University, Assiut, Egypt.
Printed ISSN 2812-5029
Online ISSN 2812-5037
Vol. 54 (3): 434- 451 (2025)
https://aunj.journals.ekb.eg

Hydrolysis of sodium borohydride using Co@Ce-UiO-66 nanocomposite as catalyst

Ahmed Abdo Hassan[1*], Mostafa Farrag[1], R. M. Gabr[1]

[1]Chemistry Department, Faculty of Science, Assiut University, Assiut, 71516 Egypt
[*] Corresponding author: ahmed_abdo@aun.edu.eg

ARTICLE INFO

Article History:
Received:2025-05-20
Accepted:2025-06-25
Online: 2025-08-28

Keywords:
MOFs,
Co@Ce-UiO-66,
Hydrolysis of $NaBH_4$,
Hydrogen production.

ABSTRACT

To address the increasing need for clean energy alternatives to fossil fuels, this study explores hydrogen generation via sodium borohydride ($NaBH_4$) hydrolysis, a safe and eco-friendly hydrogen storage material. High-performance catalysts were synthesized by modifying Ce-UiO-66 with various concentrations of cobalt nitrate ($Co(NO_3)_2{\cdot}6H_2O$) and characterized using XRD, FTIR, and nitrogen adsorption techniques. The catalysts' efficiency was evaluated in $NaBH_4$ dehydrogenation, with hydrogen generation rate (HGR) measurements highlighting the influence of Co^{2+} incorporation. Results indicate a significant activity enhancement compared to the unmodified MOF. Key parameters such as catalyst loading, $NaBH_4$ concentration, and reaction temperature were optimized, achieving a maximum HGR of 724.6 $mL{\cdot}min^{-1}{\cdot}g^{-1}$ at 50°C with 30 mg of catalyst and 0.05 M $NaBH_4$, attributed to the material's high surface area (116.2 m^2/g) and Co^{2+} active sites. Kinetic and thermodynamic analyses, including rate constants, activation energy, enthalpy, entropy, and Gibbs free energy, were conducted. The findings demonstrate the promising potential of these catalysts for advancing hydrogen energy technologies.

INTRODUCTION

The excessive reliance on fossil fuels, coupled with escalating environmental concerns, has spurred significant research efforts toward developing renewable energy solutions as sustainable replacements for traditional carbon-based fuels [1-4]. Among these alternatives, hydrogen gas stands out as a highly promising candidate, boasting an exceptional energy density of 142 MJ/kg and producing only water as a clean byproduct [5]. Hydrogen can be generated through various methods, such as water splitting or oxidation processes [6,7] including electrolysis [8-12], thermolysis, and photocatalytic water splitting [13] as well as through the utilization of phototrophic microorganisms (biohydrogen, $BioH_2$) [14]. Hydrolysis of hydrides, such as sodium borohydride ($NaBH_4$), is promising for supplying hydrogen to end users on demand [15]. Sodium borohydride ($NaBH_4$) has many advantages, including safety, affordability, relatively

high stability, and containment of 10.6 wt% of hydrogen compared to other hydrogen production methods. The hydrolysis of $NaBH_4$ can be elucidated by the following equation:

$$\mathbf{NaBH_4+2H_2O \rightarrow 4H_2+NaBO_2} \qquad \Delta \mathbf{H= -212.1\ kJ/mol} \qquad \mathbf{(1)}$$

In general, at room temperature $NaBH_4$ undergoes self-hydrolysis at an extremely slow rate [16], making the use of highly efficient catalysts essential. This process typically employs both precious and non-precious metal catalysts. Within the precious metal category, ruthenium (Ru), platinum (Pt), and palladium (Pd) represent the most widely used options [17]. However, the limited availability and high cost of these metals significantly restrict their large-scale use. Alternatively, non-precious metals have gained attention due to their affordability and abundant availability. Among these, cobalt-based catalysts have demonstrated superior catalytic activity compared to other non-precious metals [18,19]. Supporting transition metals is necessary to improve their catalytic performance and to prevent the aggregation of active species. Metal organic frameworks (MOFs) are among the most widely used supports for transition metals nanoparticles, because they are a type of porous materials that have numerous benefits such as a large surface area, substantial pore volume, low density, and various crystal structures [20-25].

In this work, Co@Ce-UiO-66 catalysts were prepared using a wet impregnation technique by incorporating varying loading percentages of ($Co(NO_3)_2{\cdot}6H_2O$) into the Ce-UiO-66 framework, aiming to enhance its catalytic performance for $NaBH_4$ dehydrogenation. The hydrogen generation rate (HGR) was measured in order to assess the effect of different loadings of Co^{2+} ions on the catalytic dehydrogenation of $NaBH_4$.

MATERIALS AND METHOD

1. Materials

1.1. Synthesis of Ce-UiO-66

Ce-UiO-66 was synthesized following an adapted protocol based on the procedure reported by Yassin et al. [26]. Initially, 1.644 g of cerium (IV) ammonium nitrate was dissolved in 3.6 mL of deionized water with stirring for 30 minutes. In a separate container, 0.332 g of terephthalic acid (BDH) was dissolved in 15.4 mL of dimethyl formamide (DMF). The cerium solution was maintained under constant stirring while the BDC solution was added dropwise, resulting in a yellow precipitate that was further stirred at room temperature for 24 hours. The solid product was then isolated via centrifugation, thoroughly washed three times with DMF followed by acetone, and finally dried at 80°C overnight.

1.2. Synthesis of x% Co@Ce-UiO-66

Co@Ce-UiO-66 was prepared via wet impregnation [27]. Specifically, 1 g of the MOF was introduced into an aqueous solution of ($Co(NO_3)_2.6H_2O$) containing the targeted loading (x = 5, and 10 wt.%). The mixture was stirred at 70 °C for approximately 2 hours, followed by drying in an oven at 100 °C for 24 h.

2.2. Characterization techniques

The structural and surface characteristics of both unmodified and modified MOFs were characterized by X-ray diffraction (XRD), Fourier-transform infrared spectroscopy (FTIR), and nitrogen physisorption (BET) analysis. XRD measurements were performed on a Philips PW 2103/100 diffractometer equipped with Cu Kα radiation (λ = 1.5418 Å), scanning across a 2θ range of 5–90° at a rate of 0.06°/min. FTIR spectra were recorded in the range of 4000–400 cm^{-1} with a resolution of 4 cm^{-1} using a Shimadzu IR-470 spectrophotometer (Japan), with samples prepared as lightly loaded KBr pellets. The surface area was determined through nitrogen adsorption-desorption isotherm analysis at 77 °K using Quantachrome gas adsorption analyzer (model 3200), using approximately 0.1 g of each catalyst in order to determine (S_{BET}) surface areas.

2.3. $NaBH_4$ hydrolysis

The hydrolysis of sodium borohydride ($NaBH_4$) was conducted in a 100 mL reaction flask under isothermal conditions, and the volume of hydrogen gas evolved (V_{H2}/mL) was measured over time (t, min) using a gasometric technique. The amount of hydrogen generated was determined based on the measured volume of water displaced from a connected liquid burette system, ensuring pressure equilibrium across the manometer. The reaction flask was immersed in a thermostatically controlled bath (30–50 °C), with a magnetic stirrer used to maintain uniform temperature throughout the reaction.

Typically, 50 mL of an aqueous $NaBH_4$ solution with concentrations ranging from 0.03 to 0.11 M was introduced into the flask. A specified mass (0.01–0.07 g) of the catalyst was then added to initiate the hydrolysis reaction. These measurements were used to construct isothermal V_{H2} vs. time profiles for each experiment. Prior to each catalytic test, the samples were mildly activated by heating at 80–100 °C for 1 hour. The hydrogen generation rate (HGR) was determined based on the equation:

$$HGR = V_{H2}\,(mL) / t\,(min) * m\,(g)$$

where m represents the total catalyst mass, t denotes the reaction duration for complete hydrolytic dehydrogenation, and V_{H2} corresponds to the total hydrogen gas volume generated.

RESULTS AND DISCUSSION

1. Characterization

1.1. XRD analysis

The XRD pattern of Ce-UiO-66, as illustrated in Fig.1 , exhibits characteristic peaks around 2θ values of 7.4°, 8.5°, 12.0°, 16.5°, 18.0°, and 25.0°, among others. The XRD diffractogram of Ce-UiO-66 confirms its cubic crystal structure, showing some characteristic peaks similar to UiO-66. The presence of slight peak shifts compared to Zr-UiO-66 suggest structural changes due to cerium incorporation. The broadening of the characteristic peaks compared to the case of Zr-UiO-66 indicates the presence of small crystallites and/or amorphous nature. The absence of any other peaks confirms the high purity of the synthesized Ce-UiO-66. The diffractogram obtained for Co@Ce-UiO-66 indicates that the addition of Co^{+2} ions didn't have any significant impact on the diffraction patterns of the pure MOF. This suggests that the added species Co^{+2} are likely well-dispersed within the MOF pores, probably in a state of an amorphous or non- non-crystalline species.

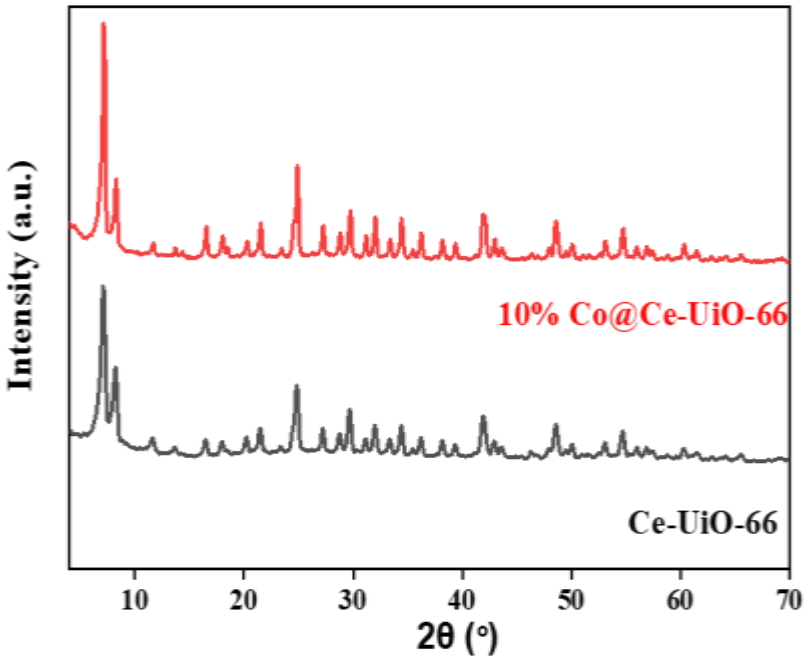

Fig. 1: XRD diffractograms obtained for Ce-UiO-66 and 10% Co@Ce-UiO-66.

1.2. FTIR analysis

The chemical compositions of Ce-UiO-66 and 10% Co@Ce-UiO-66 were analyzed using FTIR spectroscopy (Fig. 2). The spectrum of Ce-UiO-66 exhibited characteristic peaks at 3400 cm^{-1}(O–H stretching), 1650 cm^{-1} (C=O stretching), 1505 cm^{-1} (aromatic C=C stretching), and doublet bands at 1561 and 1380 cm^{-1} (asymmetric and symmetric vibrations of carboxylate groups) [28–33]. Upon cobalt modification, the 10% Co@Ce-UiO-66 spectrum displayed a broader O–H stretching band at 3390 cm^{-1}, attributed to water/hydroxyl groups from $Co(NO_3)_2 \cdot 6H_2O$. Additionally, the carboxylate vibrations shifted to 1549 and 1376 cm^{-1}, suggesting coordination between Co^{2+} ions and the organic linker. These modifications confirm the effective cobalt incorporation while preserving the Ce-UiO-66 framework structure.

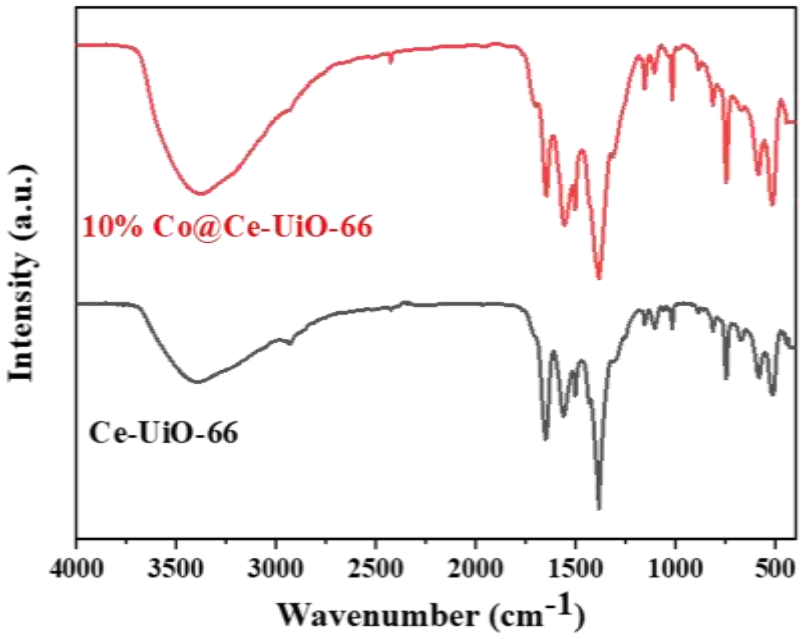

Fig. 2: FT-IR spectra obtained for Ce-UiO-66 and 10% Co@Ce-UiO-66.

3.1.3. N_2 adsorption

The texture and porous nature of both Ce-UiO-66 and 10% Co@Ce-UiO-66 samples were examined by nitrogen adsorption-desorption isotherms, as shown in Fig. 3. The isotherms for Ce-UiO-66 and Co@Ce-UiO-66 can be classified mainly as type II based on Brunauer's classification. The isotherm for Ce-UiO-66 exhibit H4 hysteresis loop, indicating narrow pores with uniform size and shape. Conversely, Co@Ce-UiO-66 displays H2 hysteresis loop, signifying the presence of ink-bottle pores [34]. The specific surface areas (S_{BET}) of these catalysts were determined applying the BET equation in the range of P/P_0 = 0.05–0.30. The BET specific surface areas are calculated to be 99.6 and 116.2 m^2 g^{-1} for Ce-UiO-66 and Co@Ce-UiO-66 respectively (Table 1). Fig. 1b shows the corresponding pore-size distribution curves, where the pore structure parameters are listed in Table 1. Specifically, total pore volumes of Ce-UiO-66 and Co@Ce-UiO-66 are 3.7 and 12.2 (cc/g)*10^{-2}, respectively. The pore radius of Ce-UiO-66 and Co@Ce-UiO-

66 are 17.3 and 26.8 **Å**, respectively. These results suggest the mesoporous structures of Ce-UiO-66 and Co@Ce-UiO-66.

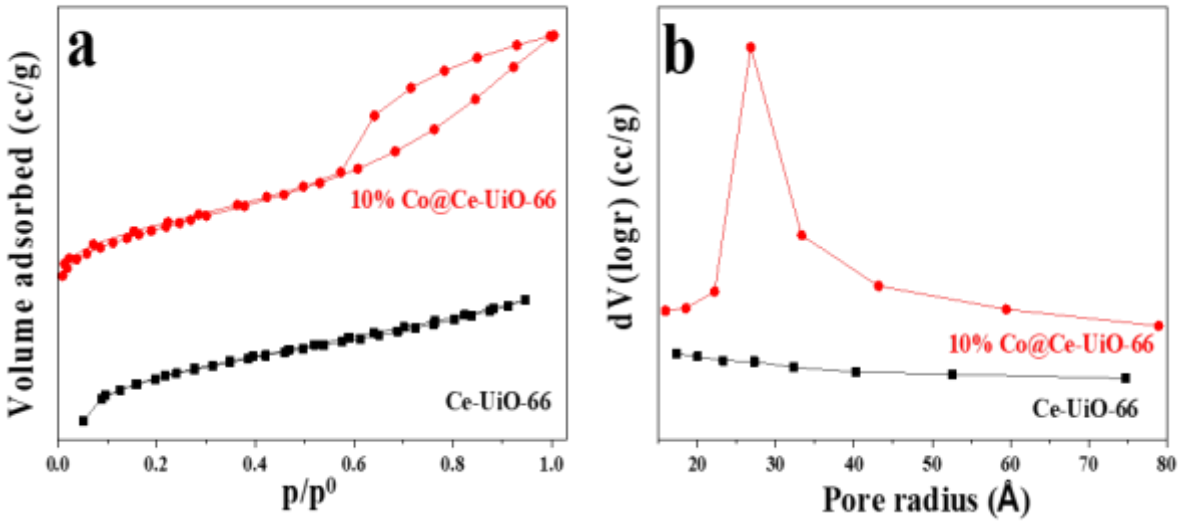

Fig. 3: a) N_2 adsorption-desorption isotherms of Ce-UiO-66 and 10% Co@Ce-UiO-66, b) Pore-size distribution for Ce-UiO-66 and 10% Co@Ce-UiO-66.

Table (1): The specific surface area S_{BET}, pore characteristics of Ce-UiO-66 and Co@Ce-UiO-66

Catalyst	Surface area (S_{BET}) (m^2/g)	Pore volume (cc/g)*10^{-2}	Pore radius (Å)
Ce-UiO-66	**99.6**	**3.7**	**17.3**
Co@Ce-UiO-66	**116.2**	**12.2**	**26.8**

2. Catalytic activity

First of all, primary experiments were conducted in order to assess the modification of Ce-UiO-66 by incorporation of Co^{2+} ions at different loading levels via dehydrogenation of sodium borohydride. The obtained histograms illustrated in Fig. 4 indicate that the above considered modification results in a noticeable reduction in the time required to produce 75 mL of H_2 upon increasing the Co^{2+} loading. Therefore, these

measurements judge the enhancement of the effect of Co^{2+} ions on the hydrolysis reaction.

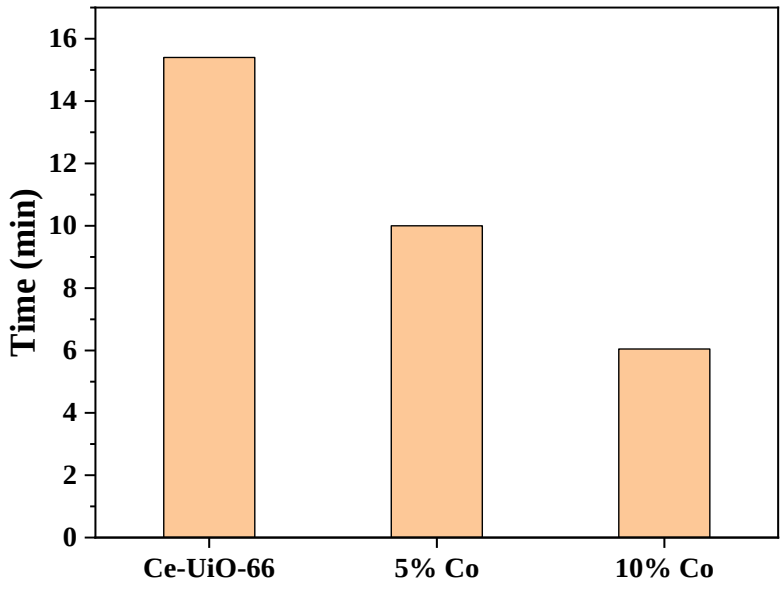

Fig.4: Histograms representing the effect of the Co loading level (5,10 wt.%) on the reaction time up to V_{75} of H_2 generated on Ce –UiO-66 and Co@Ce-UiO-66. Reaction conditions: 50 mL of $NaBH_4$ solution of 0.05 M; catalyst mass (0.03 g); and reaction temperature (30 °C).

Seeking for the different impacts, beside the fact that temperature plays an important role on the practical performance of hydrogen generation process. There are other impacts like catalyst mass and $NaBH_4$ concentration which also affect both rate and reaction order.

2.1. Effect of catalyst weight

The relation between reaction rate and the catalyst dose is a critical factor due to the available surface coverage of catalyst surface. So this relation was examined and the data obtained are illustrated in (Fig. 5). The impact of catalyst mass (0.01, 0.03, 0.05, and 0.07 g) was investigated using a 0.05 M $NaBH_4$ solution at 30 °C. The figure reveals that as the amount of catalyst is increased, the reaction time required to produce 75 mL of H_2 decreased.

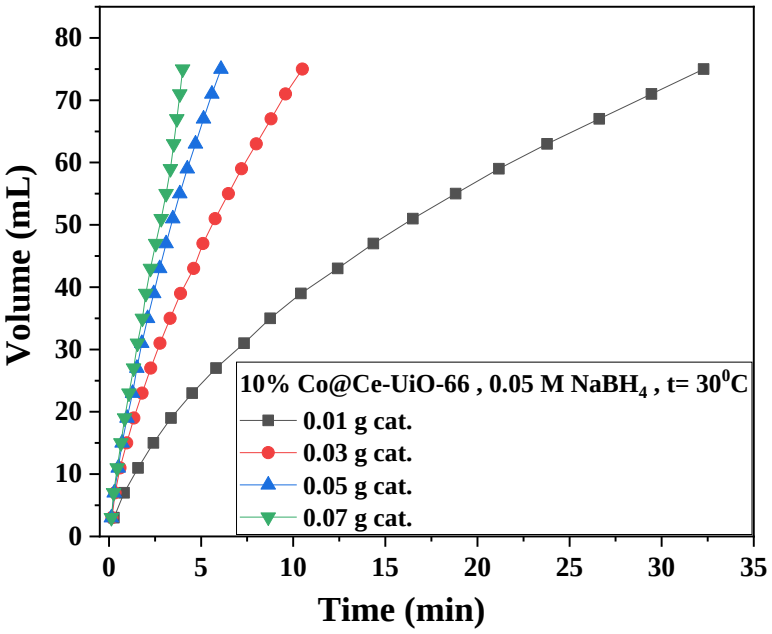

Fig. 5: V_{H2}-t plots obtained to test the influence of the catalyst mass under the following invariant reaction conditions: 50 mL of $NaBH_4$ solution of 0.05 M; and reaction temperature (30 °C).

2.2. Effect of $NaBH_4$ concentration

To investigate the effect of $NaBH_4$ concentration on the dehydrogenation kinetics, catalytic hydrolysis experiments were conducted using $NaBH_4$ solutions (0.05–0.11 M) with 0.03 g of catalyst at 30 °C. The temporal evolution of hydrogen generation is presented in Fig. 6. As can be observed from the figure, the volume of hydrogen obtained increases by increasing the concentration of $NaBH_4$ and accordingly the hydrogen production rate increases. The figure also demonstrates that the time necessary for event completion decreases upon raising $NaBH_4$ concentration.

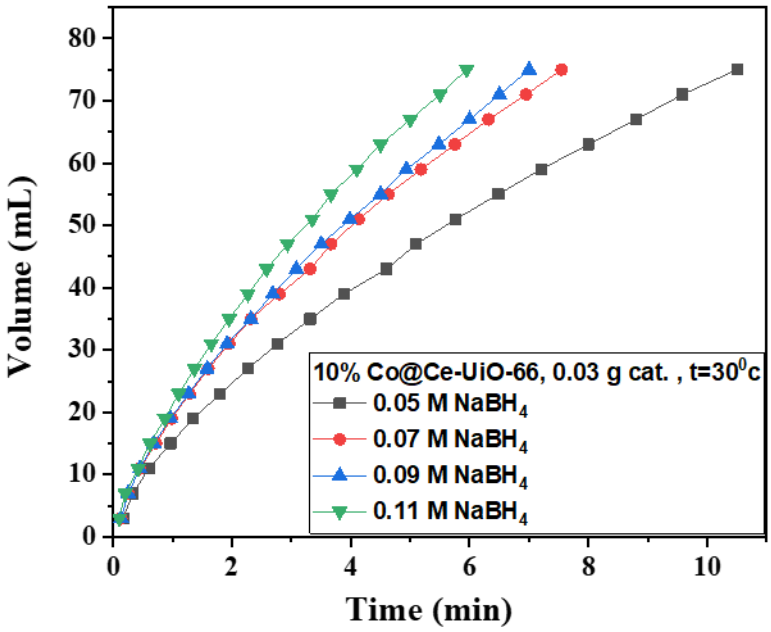

Fig. 6: V_{H2}-t plots obtained to test the influence of the $NaBH_4$ concentration under the following invariant reaction conditions: 50 mL of $NaBH_4$ solution; catalyst mass (0.03 g); and reaction temperature (30 °C).

2.3. Effect of reaction temperature

The reaction temperature plays an important role in the hydrolysis process involved in hydrogen generation (Fig. 7). In the case of $NaBH_4$ hydrolysis, the hydrogen production rate rises as the reaction temperature increases (Fig. 7). This is explained by the fact that at higher temperatures, the gas molecules have more kinetic energy and hence more collision rate. Accordingly, experimental findings demonstrate the fact that the rate of hydrogen generation is highly influenced by the reaction temperature.

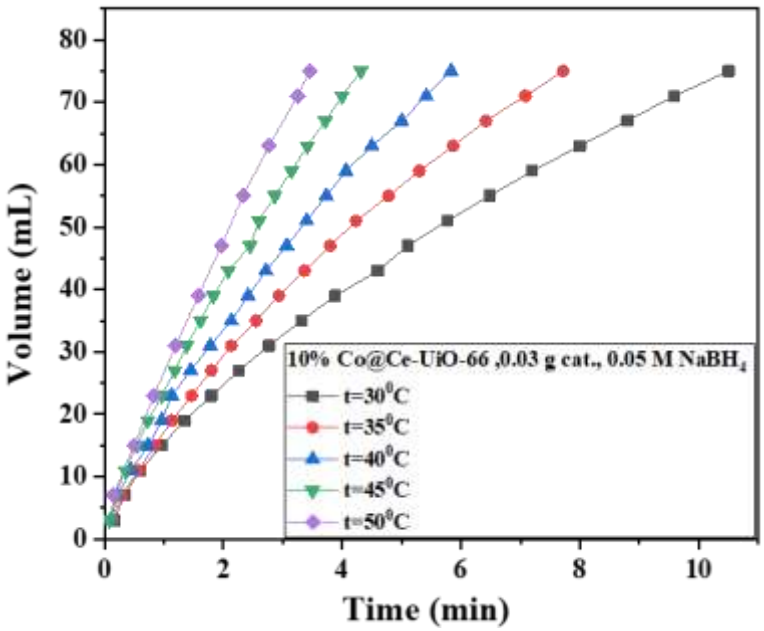

Fig. 7: V_{H2}-t plots obtained to test the influence of the reaction temperature under the following invariant reaction conditions: 0.05 M $NaBH_4$; catalyst mass (0.03 g).

3. Catalytic dehydrogenation kinetic and thermodynamic parameters:

To determine the kinetic and thermodynamic parameters of the catalytic dehydrogenation reaction, the obtained V_{H_2} –t data were converted into [$NaBH_4$]–t plots, from which ln (a–x)–t plots (Fig. 8a) were generated to determine the reaction order (n) using a trial-and-error method. The rate constants (k) were calculated from the slope of the linear ln (a–x)–t plots. The variation of the calculated first order rate constants within the temperature range 30-50 $^{\circ}$C were studied through the following Arrhenius equation (2) in its linear form is displayed in Fig. 8b:

$$\ln k = \ln A - E_a/RT \quad (2)$$

Where k, A, R, T are the rate constant of reaction, pre-experimental factor, universal gas constant (0.008314 KJ mol $^{-1}$ K^{-1}), and absolute reaction temperature, respectively. The activation energy (Ea) for the catalyzed reaction was calculated from the graphical representation of ln k versus 1/T as shown in **Fig. 8b** and was found to be 45.9 kJ/mol (R^2= 0.998).

The enthalpy (ΔH) and entropy (ΔS) changes accompanying the catalytic reaction were calculated by applying the Eyring equation (3):

$$k = k_B T/h \; e^{\Delta S/R} \; e^{-\Delta H/RT} \quad (3)$$

where k, k_B and h are the rate constant, Boltzmann constant (1.381 X 10^{-23} J/K), and Plank's constant (6.626 x10^{-34} J.s), respectively. Moreover, the free energy of activation can be obtained by equation (4):

$$\Delta G = \Delta H - T\Delta S \quad (4)$$

where ΔS and ΔG are the entropy, free energy of activation, while T is the absolute temperature and ΔH is the enthalpy change for $NaBH_4$ dehydrogenation (-212.1 kJ/mol).

The results given in Table (2) reveal that the calculated ΔG and ΔH assume negative values, whereas ΔS assumes positive values. This indicates that the catalytic dehydrogenation of $NaBH_4$ on Co@Ce-UiO-66 is thermodynamically feasible.

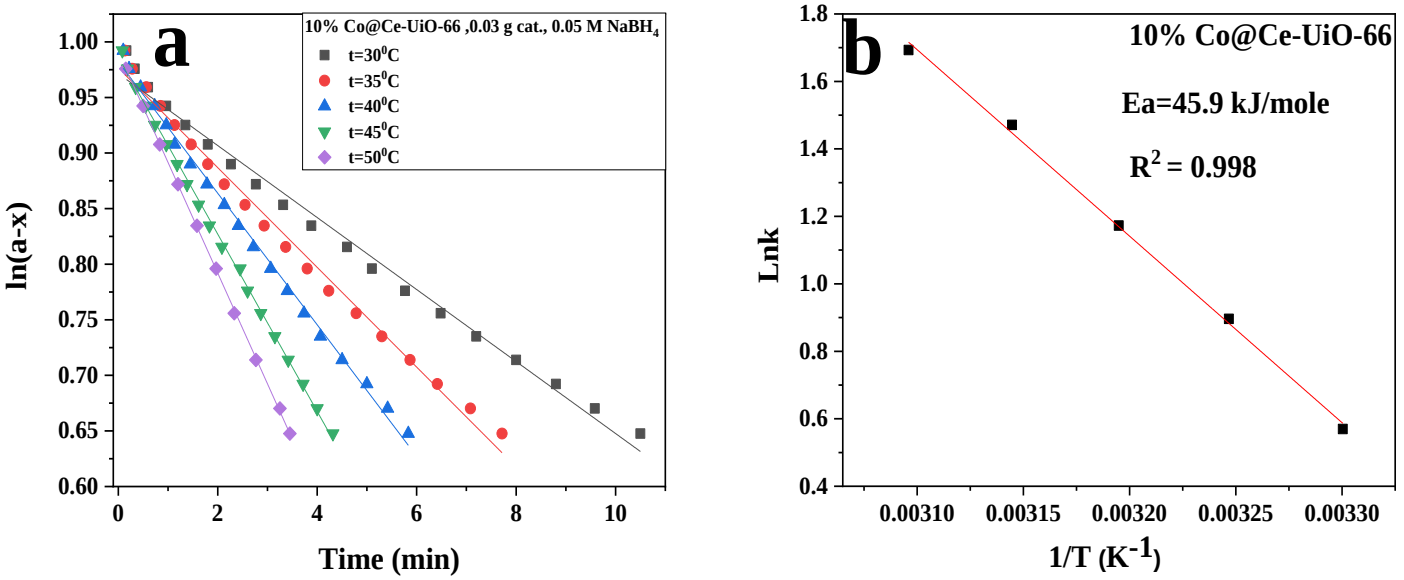

Fig. 8: a) ln (a-x) versus time plots constructed for the $NaBH_4$ dehydrogenation reaction on Co@Ce-UiO-66 at different reaction temperatures (30-50°C), b) Arrhenius plot (ln k versus 1/T) constructed for the $NaBH_4$ dehydrogenation reaction on Co@Ce-UiO-66.

Table 2: The rate constant, activation energy, enthalpy change, the entropy and free energy of activation for the catalytic $NaBH_4$ dehydrogenation reaction.

T (^{0}K)	k (min^{-1})	Ea (kJ.mol^{-1})	ΔH (kJ.mol^{-1})	ΔS (kJ.K^{-1}.mol^{-1})	ΔG (kJ.mol^{-1})
303	0.032	45.9	-212.1	0.97	-81.81
308	0.045			0.96	-83.58
313	0.059			0.947	-84.31
318	0.08			0.933	-84.59
323	0.1			0.92	-85.06

4. Reaction mechanism

Building upon established studies of the $NaBH_4$ hydrolysis mechanism [35], the proposed reaction pathway involves the diffusion of $NaBH_4$ and H_2O molecules into the porous network of Ce-UiO-66, where they become adsorbed onto the uniformly dispersed Co^{2+} active sites within the MOF's framework. The catalytic process initiates when Co^{2+} ions coordinate with BH_4^- anions, inducing electron redistribution that weakens and

polarizes the B-H bonds. This activation renders the boron center more susceptible to nucleophilic assault by water molecules.

The hydrolysis progresses through a sequential mechanism: initial water attack at the boron atom leads to heterolytic cleavage of a B-H bond, releasing the first H_2 molecule while generating a $BH_3(OH)^-$ intermediate that remains bound to the catalyst surface. This intermediate then undergoes three successive hydrolysis cycles, with each step cleaving an additional B-H bond and liberating one H_2 molecule per cycle. The reaction culminates in the complete conversion of the borohydride species to the thermodynamically stable final product tetrahydroxyborate ions $[B(OH)_4]^-$, which might be formed due to hydrolysis of metaborate ions BO_2^-, while regenerating the active sites for subsequent catalytic cycles.

This multi-step mechanism highlights the crucial role of the MOF's porous architecture in facilitating reactant accessibility to the active centers, while the Co^{2+} sites serve to lower the activation energy barrier through selective polarization of key bonds. The stepwise nature of the process ensures controlled hydrogen evolution, making the system particularly suitable for practical hydrogen storage applications where regulated gas release is essential.

5. Catalyst recyclability

To evaluate the catalyst's reusability, additional experiments were performed and the obtained results are presented in (Fig. 9). The outcomes reveal that 10% Co@Ce-UiO-66 maintains its catalytic efficiency over four successive cycles with minimal performance decline. This indicates excellent recyclability and suggests that the material remains structurally intact without significant degradation during use. The stable nature of 10% Co@Ce-UiO-66 enables its repeated application in various catalytic reactions, reducing the need for frequent replacement. Moreover, its reusability helps minimize waste associated with catalyst disposal, supporting environmentally sustainable practices.

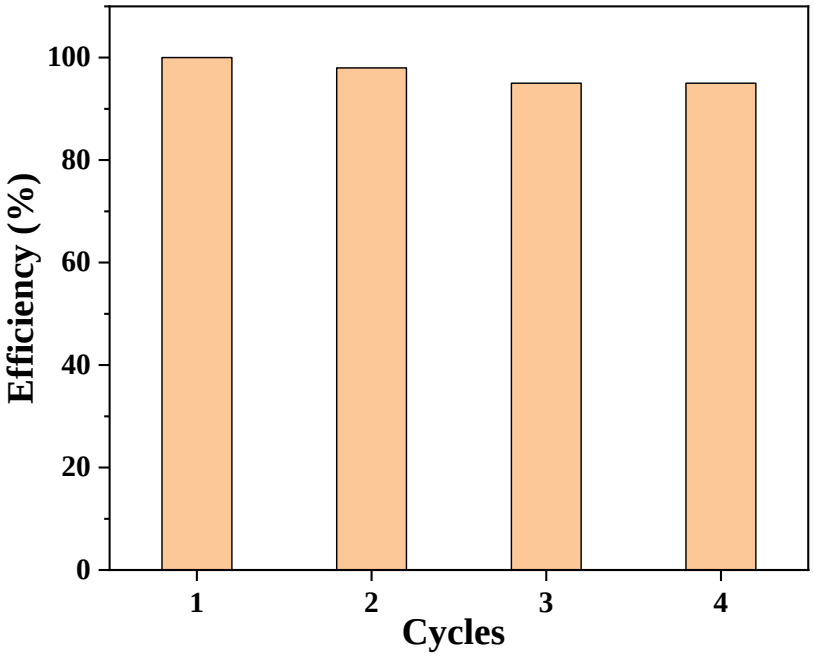

Fig. 9: Reusability effect on the performance of 10% Co@Ce-UiO-66 catalyst. Reaction conditions: 50 mL of $NaBH_4$ solution of 0.05 M; catalyst mass (0.03 g); and reaction temperature (30 °C).

Table 3 compares HGR values measured on our present catalysts with some of those reported in the literature. 10% Co@Ce-UiO-66 at 50°C gives higher HGR values than other catalysts. The comparison reveals that our catalysts are quite competitive and even superior to the reported catalysts such as Co powder, and Raney Co [36]. Co-La-Zr-B [37]. Co/MWCNTS-20 [38], Co-B/C [39], CoB@ZIF-8 [40] and Ce-UiO-66 [41].

Table 3: HGR values measured using our present catalysts and literature-reported ones.

Catalyst	Catalyst wt.	Reaction conditions	HGR ($mL.min^{-1}.g^{-1}$)	Ref.
Co powder	2.5%	1 wt.% $NaBH_4$, 10 wt.% NaOH, 20 ^0C	126.2	[36]
Raney Co	2.5%	1 wt.% $NaBH_4$, 10 wt.% NaOH, 20 ^0C	267.5	[36]
Co-La-Zr-B	0.05%	0.5 wt.% $NaBH_4$, 20 wt.% NaOH, 20 ^0C	216	[37]
Co/MWCNTS-20	0.15%	1 wt.% NaBH4, 35^0C	410	[38]
Co-B/C	2.5%	1 wt.% $NaBH_4$, 5 wt.% NaOH, 25 ^0C	166	[39]
CoB@ZIF-8	10 mg	1.67 wt.% $NaBH_4$,5 wt.% NaOH, 35^0C	453.6	[40]
Ce-UiO-66	50 mg	0.05 M $NaBH_4$, 30 ^0C	97.4	[41]
10 % Co@Ce-UiO-66	50 mg	0.05 M $NaBH_4$, 30 ^0C	250	This study
10 % Co@Ce-UiO-66	30 mg	0.11 M $NaBH_4$, 30 ^0C	420.2	This study
10 % Co@Ce-UiO-66	30 mg	0.05 M $NaBH_4$, 35^0C	324.3	This study
10 % Co@Ce-UiO-66	30 mg	0.05 M $NaBH_4$, 40 ^0C	428.8	This study
10 % Co@Ce-UiO-66	30 mg	0.05 M $NaBH_4$, 45 ^0C	471.7	This study
10 % Co@Ce-UiO-66	30 mg	0.05 M $NaBH_4$, 50 ^0C	724.6	This study

CONCLUSIONS

In summary, Co@Ce-UiO-66 catalysts were successfully prepared using a wet impregnation technique, where Ce-UiO-66 was treated with various loadings (5 and 10 wt. %) of $Co(NO_3)_2 \cdot 6H_2O$. The resulting materials were characterized using XRD, FTIR, and N_2 sorption techniques, and their catalytic performance was assessed in the dehydrogenation of sodium borohydride. The catalyst demonstrated excellent efficiency, rapid reaction time, minimal catalyst usage, and low metal leaching. Specifically, 10% Co@Ce-UiO-66 exhibited a high hydrogen generation rate (HGR) of 724.6 $mL.min^{-1}.g^{-1}$ at 50^oC, even when using a low-concentration $NaBH_4$ solution (50 mM). The kinetic analysis of the activity data were studied and the results indicate the first order kinetic behavior at low concentration of $NaBH_4$. The activation energy was found to be 45.9 KJ/mole. Furthermore, the observed trend in entropy, activation energy, enthalpy, and free energy confirms that the hydrolysis reaction is spontaneous, feasible, and exothermic in nature. Moreover, the materials exhibited notable recyclability, maintaining high catalytic activity and consistent performance over four consecutive cycles with minimal

loss in efficiency. This stability highlights their potential for energy-related applications and suitability for large-scale industrial use.

Acknowledgment

This work was financially supported by Assiut University, Egypt.

REFERENCES

[1] Z. Zhang, G.W. Huber, Catalytic oxidation of carbohydrates into organic acids and furan chemicals, Chem. Soc. Rev., 47 (2018) 1351-1390.

[2] D.S. Scott, Conventional wishdom, Int. J. Hydrogen Energy, 6 (2005) 569-577.

[3] J.N. Armor, Environmental catalysis, Appl. Catal. B: Environ., 1 (1992) 221-256.

[4] E. Lox, B. Engler, Environmental catalysis mobile sources, in, Wiley Online Library, 1999, pp. 1-117.

[5] P. Brack, S.E. Dann, K. G. U. Wijayantha, Heterogeneous and homogenous catalysts for hydrogen generation by hydrolysis of aqueous sodium borohydride (NaBH4) solutions, Energy Sci. Eng. 3 (2015) 174-188.

[6] M. M. Najafpour, M. Z. Ghobadi, B Sarvi, S. Madadkhani, D. S. Jafarian, P Rafighi, et al, Polypeptide and Mn-Ca oxide: toward a biomimetic catalyst for water-splitting systems, Int. J. Hydrogen Energy, 41(2016) 5504-5512.

[7] M. N. Iqbal, A. F. Abdel-Magied, H. N. Abdelhamid, P. Olsen, A. Shatskiy, X. Zou, et al, Mesoporous ruthenium oxide: a heterogeneous catalyst for water oxidation. ACS Sustain. Chem. Eng. 5(11) (2017) 9651-9656.

[8] J. Zhang, R. Cui, X. Li, X. Liu, W. Huang, A nanohybrid consisting of $NiPS_3$ nanoparticles coupled with defective graphene as a pH-universal electrocatalyst for efficient hydrogen evolution, J. Mater. Chem., 5 (2017) 23536-23542.

[9] Y. Cui, C. Zhou, X. Li, Y. Gao, J.Zhang, High performance electrocatalysis for hydrogen evolution reaction using nickel-doped CoS_2 nanostructures: experimental and DFT insights, Electrochim. Acta, 228 (2017) 428-435.

[10] Y. Cui, R. Zhang, J. Zhang, Z. Wang, H. Xue, W. Mao, et al, Highly active and stable electrocatalytic hydrogen evolution catalyzed by nickel, iron doped cobalt disulfide@reduced graphene oxide nanohybrid electrocatalysts, Mater. Today Energy, 7 (2018) 44-50.

[11] M.M. Najafpour, S. Mehrabani, R. Bagheri, Z. Song, J.-R. Shen, S. I. Allakhverdiev, An aluminum/cobalt/iron/nickel alloy as a precatalyst for water oxidation, Int. J. Hydrogen Energy, 43 (2018) 2083-2090.

[12] G. Azadi, R. Bagheri, R. Bikas, Y. Mousazade, J. Cui, Z. Song, et al, A transparent electrode with water-oxidizing activity,Int. J Hydrogen Energy, 43 (2018) 22896-22904.

[13] J. Zhang, F. Feng, Y. Pu, X. Li, C. H. Lau, W. Huang, Tailoring the porosity in iron phosphosulfide nanosheets to improve the performance of photocatalytic hydrogen evolution, Chem. Sus. Chem., (2019).

[14] K. Bolatkhan, B. D. Kossalbayev, B. K. Zayadan, T. Tomo, T. N. Veziroglu, S. I. Allakhverdiev. Hydrogen production from phototrophic microorganisms: reality and perspectives, Int. J. Hydrogen Energy, 44 (2019) 5799-5811.

[15] N. Patel, A. Miotello, Progress in Co-B related catalyst for hydrogen production by hydrolysis of boron-hydrides: a review and the perspectives to substitute noble metals, Int. J. Hydrogen Energy 40 (2015) 1429-1464.

[16] H.N. Abdelhamid, A review on hydrogen generation from the hydrolysis of sodium borohydride, Int. J. Hyrogen Energy 46 (2021) 726–765.

[17] M. Dragan, Hydrogen storage in complex metal hydrides $NaBH_4$: hydrolysis reaction and experimental strategies, Catalysts 12 (2022) 356.

[18] U. B. Demirci , O. Akdim, J. Hannauer, R. Chamoun, P. Miele, Cobalt, a reactive metal in releasing hydrogen from sodium borohydride by hydrolysis: a short review and a research perspective, Sci. China Chem. 53(9) (2010) 1870 - 1879.

[19] Ö. Şahin, D. Kilinç, C. Saka. Hydrogen production by catalytic hydrolysis of sodium borohydride with a bimetallic solid- state Co- Fe complex catalyst, Sep Sci. Technol. 50 (2015) 2051- 2059.

[20] H.N. Abdelhamid, Z. Huang, A.M. El-Zohry, H. Zheng, X. Zou, A Fast and Scalable Approach for Synthesis of Hierarchical Porous Zeolitic Imidazolate Frameworks and One-Pot Encapsulation of Target Molecules, Inorg. Chem. 56(15) (2017) 9139–9146.

[21] Y. Yang, K. Chen , J.Z. Lin, Y. Zhou ,Q.Y. Liu, C. Hang , H.N. Abdelhamid, Z.Q. Zhang, H. Chen ,A Zn-MOF constructed from electron-rich π-conjugated ligands with an interpenetrated graphene-like net as an efficient nitroaromatic sensor, RSC Adv. 6 (2016) 45475–45481.

[22] H.N. Abdelhamid , X. Zou, Template-free and room temperature synthesis of hierarchical porous zeolitic imidazolate framework nanoparticles and their dye and CO_2 sorption, Green Chem. 20 (2018) 1074–1084.

[23] A.F. Abdel-Magied, H.N. Abdelhamid, R.M. Ashour, X. Zou, K. Forsberg, Hierarchical porous zeolitic imidazolate frameworks nanoparticles for efficient adsorption of rare-earth elements, Microporous Mesoporous Mater. 278 (2019) 175–184.

[24] Z. Chen, S. L. Hanna, L. R. Redfern, D. Alezi, T. Islamoglu, and O. K. Farha, Reticular chemistry in the rational synthesis of functional zirconium cluster-based MOFs, Coord. Chem. Rev. 386 (2019) 32–49.

[25] H.N. Abdelhamid, Surfactant assisted synthesis of hierarchical porous metal-organic frameworks nanosheets, Nanotechnol. 30 (2019) 435601.

[26] J.M. Yassin, A.M. Taddesse, M.S. Sanchez, Room temperature synthesis of high-quality Ce (IV) -based MOFs in water, Microporous Mesoporous Mater. 324 (2021) 111303.

[27] F.T. Alshorifi, D.E. Tobbala, S.M. El-Bahy, M.A. Nassan, and R.S. Salama, The role of phosphotungstic acid in enhancing the catalytic performance of UiO-66 (Zr) and its applications as an efficient solid acid catalyst for coumarins and dihydropyrimidinones synthesis, Catal. Commun. 169 (2022) 106479.

[28] X. Liao, X. Wang, F. Wang, Y. Yao, S. Lu, Ligand Modified Metal Organic Framework UiO-66: A Highly Efficient and Stable Catalyst for Oxidative Desulfurization, J Inorg. Organomet. Polym. Mater. 31 (2021) 756–762.

[29] F. Khosravi, M. Gholinejad, J.M. Sansano, R. Luque, Bimetallic Fe–Cu metal organic frameworks for room temperature catalysis, Appl. Organomet. Chem. 36 (2022) 6749.

[30] S. Subudhi, G. Swain, S.P. Tripathy, K. Parida, UiO-66-NH_2 Metal-Organic Frameworks with Embedded MoS_2Nanoflakes for Visible-Light-Mediated H_2 and O_2 Evolution, Inorg. Chem. 59(14) (2020) 9824–9837.

[31] A. Raghi, K. Ghani, M. Jafari, Modification of UiO-66 for removal of uranyl ion from aqueous solution by immobilization of tributyl phosphate, J. Chem. Sci. 133 (2021) 14.

[32] A.S. Elsherbiny, A. Rady, R.M. Abdelhameed, A.H. Gemeay, Efficiency and selectivity of cost-effective Zn-MOF for dye removal, kinetic and thermodynamic approach, Environ. Sci. Pollut. Res. 30 (2023) 106860–106875.

[33] N. Riezzati, Y.K. Krisnandi, A. Zulys, Metal organic frameworks of lanthanum and iron using BDC linker as catalysts for glucose conversion into 5-hydroxymethylfurfural (5-HMF), IOP Conf. Ser.: Mater. Sci. Eng. 902 (2020) 012044.

[34] G. Leofanti, M. Padovan, G. Tozzola, B. Venturelli, Surface area and pore texture of catalysts, Catal. Today 41 (1998) 207-219.

[35] U.B. Demirci, P. Miele, Reaction mechanisms of the hydrolysis of sodium borohydride: a discussion focusing on cobalt-based catalysts, C. R. Chim. 17 (2014) 707–716.

[36] B. H. Liu, Z. P. Li, S. Suda, Nickel- and cobalt-based catalysts for hydrogen generation by hydrolysis of borohydride, J. Alloys Compd. 415 (2006) 288-293.

[37] M. H. Loghmani M. H., A. F. Shojaei Synthesis and characterization of Co-La-Zr-B quaternary amorphous nano alloy: kinetic study for hydrogen generation from hydrolysis of sodium borohydride, J. Alloys Compd. 580 (2013) 61-66.

[38] K. Narasimharao, B.M. Abu-Zied, S.Y. Alfaifi, Cobalt oxide supported multi wall carbon nanotube catalysts for hydrogen production via sodium borohydride hydrolysis, Int. J. Hydrogen Energy 46(9) (2021) 6404–6418.

[39] D. Xu, P. Dai, X. Liu, Carbon-supported cobalt catalyst for hydrogen generation from alkaline sodium borohydride solution, J. Power Sources 182 (2008) 616-620.

[40] Q. Li, W. Yang, F. Li, A. Cui, J. Hong, Preparation of CoB/ZIF-8 supported catalyst by single step reduction and its activity in hydrogen production, Int. J. Hydrogen Energy 43 (2018) 271–282.

[41] A. Abdo Hassan, M. Farrag, R. M. Gabr, Synthesis and characterization of functionalized cerium and zirconium metal-organic frameworks as novel solid acid catalysts for hydrogen generation, Egypt. J. Chem. 68(5) (2025) 179 – 192.